JOURNAL OF COMPUTATIONAL PHYSICS 6, 219–236 (1970)

The Numerical Integration of the Nonlinear Shallow-Water Equations with Sloping Boundaries

ANITA SIELECKI

Department of Meteorology, Hebrew University, Jerusalem, Israel

AND

M. G. WURTELE

Department of Meteorology, University of California, Los Angeles, California 90024

Received December 8, 1969; revised February 27, 1970

The nonlinear shallow-water equations in a rotating frame are integrated numerically over a sloping bottom with free lateral boundary conditions in such a way that the fluid determines its own level. Three different finite-difference schemes are tested and found to give equivalent results. The results are compared with nonlinear analytic solutions in one and two dimensions, and a high order of accuracy is achieved. The techniques used could be of importance in the operational forecasting of storm surges at irregular coast lines.

The "shallow-water" equations of fluid motion for a rotating frame, the derivation of which may be found in a variety of texts, for example [1], may be written as follows:

$$\begin{aligned} \frac{\partial \mathbf{v}}{\partial t} &= -\mathbf{v} \cdot \nabla \mathbf{v} - g \nabla \eta - f \mathbf{k} \times \mathbf{v}, \\ \frac{\partial \eta}{\partial t} &= -\nabla \cdot [(h(x, y) + \eta)\mathbf{v}] \equiv -\nabla \cdot (\xi \mathbf{v}). \end{aligned} \tag{1}$$

Here $\mathbf{v}$ is the horizontal velocity vector, η the displacement from equilibrium of the free surface, $h(x, y)$ the variable depth of the bottom below equilibrium water level, $\xi = h + \eta$ the depth of the fluid, g the acceleration of gravity, f the coriolis parameter, and $\mathbf{k}$ a unit vector in the vertical. Figure 1 shows the geometric configuration.

These equations have the property that the boundary conditions at the free surface and at the bottom have already been satisfied in the derivation of the equations themselves. In an arbitrary configuration, such as that of Fig. 1, for

example, *only* Eqs. (1) have to be solved, given a set of initial conditions, and the fluid determines its own level at every point of space and time. Examples of theoretical studies involving a sloping bottom without lateral boundary conditions are those of Ball [2], Stoker [3], and Carrier and Greenspan [4]. Given the nonlinearity of the equations and the way in which $h(x, y)$ enters, it is not surprising that only very special cases are amenable to analytic methods.

When computational methods have been used with these equations, it has been customary to make for ease of treatment by introducing artificial vertical walls along grid lines, at which the supplementary condition $u = 0$ or $v = 0$ is applied. This has been done extensively, for example, in storm-surge forecast

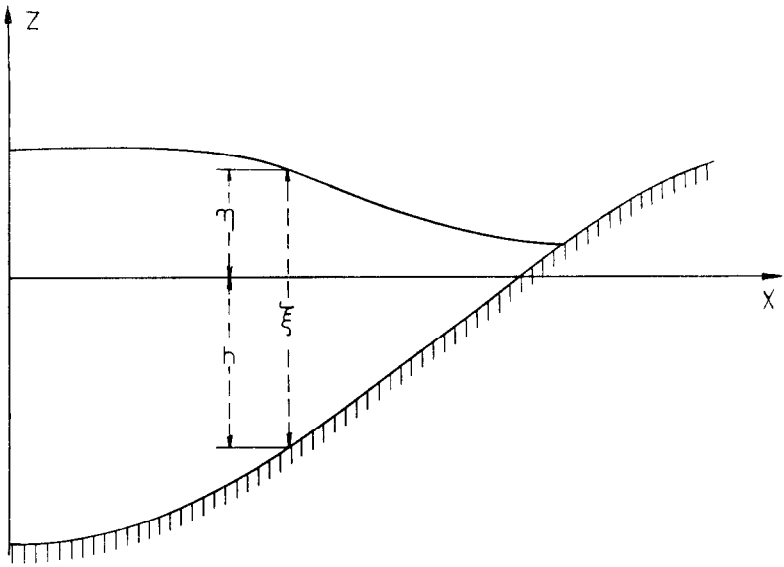

FIG. 1. Geometric configuration and notation for the present study. The y-direction is into the paper.

programs, where the linearized version of (1) is used, for the most part. In the storm surge the practical concern lies entirely in the values of the variables near the boundaries, and it is thus of importance to represent in some detail the natural shape of the coast—bays, promontories, estuaries, etc. A coast with varying curvature must, according to the usual formulation, be represented by a boundary of short segments of vertical walls meeting orthogonally—a many-cornered, totally-reflecting boundary, which produces highly undesirable computational effects precisely in the region where accuracy is desired. This problem is discussed, for example, by Platzman [5, pp. 36–37]. Reid and Bodine [6] have computed

surges in Galveston Bay using vertical boundaries which may be moved, depending on the height of the water at the boundary. These are empirically-oriented computations which attempt to validate their techniques by reference to field measurements of the tides or surges.

We present in this paper a systematic computational study using no lateral boundary conditions, in which the dynamics of the fluid under Eqs. (1) determines the position of the free surface on the sloping boundary at each time step. There exist analytical solutions—or solutions computed by the entirely independent method of characteristics—in both one and two dimensions which provide sufficient verification of the accuracy of our techniques.

Most of these analytic solutions are concerned with the tendency of the nonlinear shallow-water equations to steepen wavefronts until a vertical slope is established, at which point the equations cease to have physical meaning. Our computational procedures must therefore be able to represent this mathematical phenomenon, which for want of a better name we shall call "wave-breaking."

Obviously any viable difference scheme for this highly nonlinear system must have effective control of the energy. We have tested three schemes. One, the Lax-Wendroff as modified by Richtmyer [7], is well known and has been used before in connection with these equations (see, for example, [8]). A second is derived according to the principle of energy conservation as formulated by Arakawa [9]. The third is a simpler scheme, economical in regard to computer time, in which we relied on the quasi-implicit character of the difference equations to stabilize the computation. The difference equations for all schemes are written out in full in Appendix A. It will be noted that the coriolis term is incorporated in each case. This was set equal to zero for all experiments except Experiment 6, although the dimensional scales of the first five experiments are such that it would in any case be nonfunctional.

Experiment 1

This was designed to test the comparative behavior of the three schemes. A one-dimensional cosine wave in the free surface is imposed as an initial condition:

$$\eta(x, 0) = 0.1\, h_0 \cos \frac{2\pi x}{L}$$
$$u(x, 0) = 0$$

with vertical walls at $x = 0, L$ and constant depth h_0. The linear period of the oscillation is about 110 time steps. The results are depicted in Fig. 2. By two linear periods the slope of the surface has become quite steep, and becomes approximately vertical by 280 time steps. During this computation the three schemes agree very closely; in fact, we may say that they produce equivalent results so long as the equations (1) themselves have physical meaning. The total

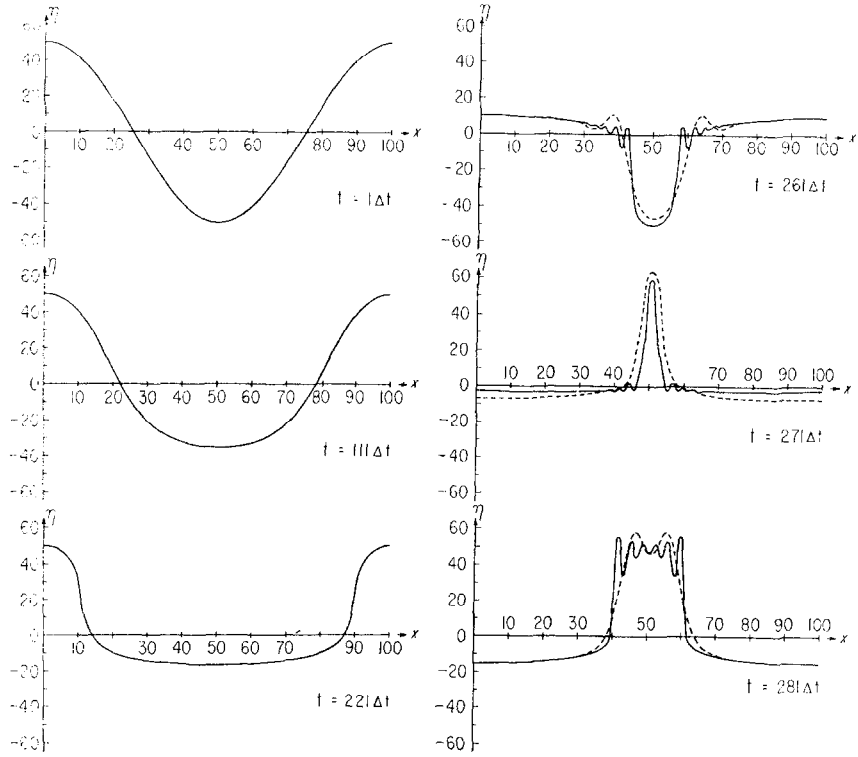

FIG. 2. Profile of the free surface at different times in the free oscillation in a one-dimensional basin of constant depth. For this computation $\eta_0/h = 0.1$ (Experiment 1). ——— Scheme II; - - - - - - - - Schemes I and III.

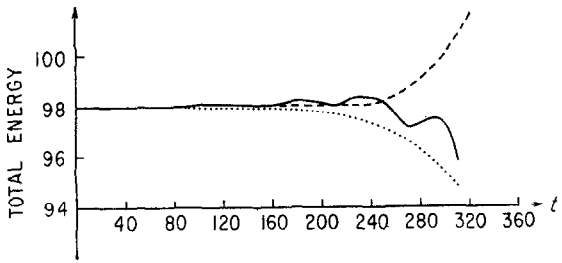

FIG. 3. Total energy of a mass of water oscillating freely in a basin of constant depth (Experiment 1). Time is measured in units of Δt. Compare Fig. 2. . . . . Scheme I; ——— Scheme II; - - - - - - - - Scheme III.

energies of the fluid, as computed by each scheme, are plotted in Fig. 3. Up to the time the computations become meaningless, the energies differ from each other and from the initial value by less than two percent.

Experiment 2

This is the computation of a simple wave advancing into still water of constant depth from the point $x = 0$:

$$\eta(0, t) = \eta_0 \sin(\Omega t - \pi). \tag{2}$$

According to the theoretical calculations of Stoker [3], this wave will break at time

$$t_B = \frac{1}{\Omega}\left(\frac{2}{3}\frac{h}{\eta_0} + \pi\right),$$

and the coordinate of the point of vertical tangency to the free surface at this time will be

$$x_B = t_B \sqrt{gh} - \tfrac{1}{2}\lambda,$$

where λ is the wavelength of the incident wave. In the numerical computations we used an incident wave of length $100\,\Delta s$ with a linear period of $145\,\Delta t$. The ratio η_0/h, which may be thought of as the measure of nonlinearity, was taken as 0.1. The corresponding values for the breaking wave are then

$$t_B \doteq 226\,\Delta t,$$
$$x_B \doteq 108\,\Delta s.$$

The results are presented in Fig. 4. At time step 114 the wave is still almost a pure sine wave; after 40 more time steps the front has begun to steepen; and time step 224 is just about breaking time. It is seen that the three computational schemes agree very well with each other and with the theory. (Even the "parasitic waves" in the wake of the steepening front are quite similar in the three schemes.) It may further be noted that the amplitude of the wave remains unchanged, in accordance with the theory.

With this background it is possible to have sufficient confidence to proceed to the computations using a sloping bottom and no lateral boundaries. The computation of these models is quite delicate. For some grid points, the depth ξ is positive ("underwater" points), and these can be treated in the usual manner. For points beyond the shore line, however, the depth ξ is negative ("underground" points), whence $\sqrt{g\xi}$ is imaginary, and the equations are exponentially unstable to the perturbations introduced by truncation. In general, our procedure is to set all variables equal to zero at points for which ξ does not exceed some very

small positive quantity determined by the accuracy of the computation. Some of the very stringent tests required a slight modification of this procedure, the details of which are relegated to Appendix B.

For the following experiments, Schemes II and III were used. Since the differences were consistently negligible, only the results of Scheme III are shown.

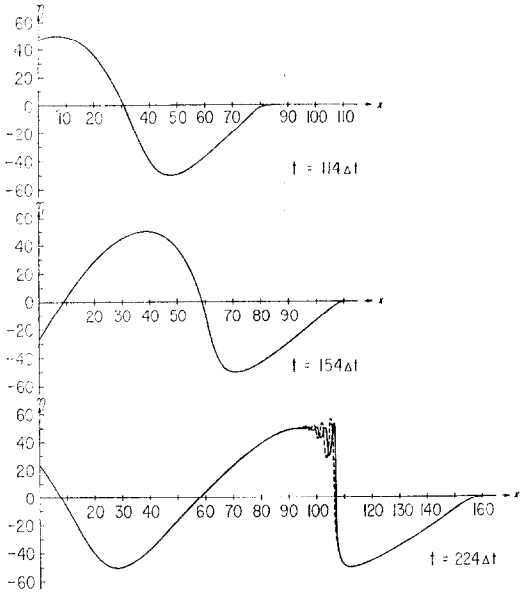

FIG. 4. The simple wave: profile of an incident sine wave propagating into quiet water of constant depth. For this computation $\eta_0/h = 0.1$; the linear period of the wave is 145 Δt; and the wavelength is 100 Δs (Experiment 2). ——— Scheme II; - - - - - - - Schemes I and III.

Experiment 3

The case of a bottom with constant slope is theoretically tractable. The incident wave (2) is imposed, as in Experiment 2, but now the sloping bottom favors the early breaking of the wave, which occurs before any perturbation has reached the shore line (see Fig. 5). The parameters of this experiment were chosen to conform to those of Stoker's computations by the method of characteristics [3, p. 76]. It is evident that the wave breaks before one-half wavelength has entered the field. The relevant parameters are

$$\eta_0/h_M = 0.2,$$
$$\tan \alpha = 0.4 \frac{2\pi}{\lambda} h_M,$$

where h_M is the depth at $x = 0$ and $\tan \alpha$ is the constant bottom slope. With these parameters, Stoker's dimensionless values for the time and position of breaking become:

$$t_B \doteq 228\, \Delta t,$$

$$x_B \doteq 40\, \Delta s.$$

The two computations, by entirely different methods, are in satisfactory agreement.

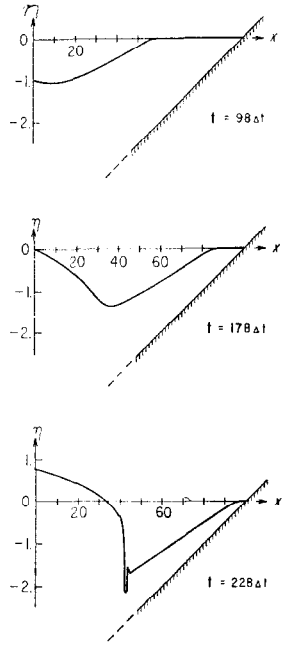

FIG. 5. Profile of an incident sine wave propagating into quiet water with a bottom of constant slope. For this computation $\eta./h_M = 0.2$. See text for further specification of parameters (Experiment 3).

Experiment 4

Here we have chosen a bottom of parabolic shape, for which no analytic solution exists. For comparison with Experiment 3, we took the same mean slope and the same incident wave. The results are presented in Fig. 6. The perturbation reaches the shore at time step 198, and the wave breaks at time step 288. Thus the curvature of the bottom has delayed the breaking time by about 23% over that of the previous experiment with the same mean slope. This makes physical sense. It is commonly observed that the rush of water down the shore toward

the oncoming wave accelerates the breaking time [3, p. 63]. For the first 262 time steps of the present experiment, the trough of the wave lies over the part of the bottom with slope *less* than the mean. From that time on, the more rapid downward rush of water along the coast then produces wave-breaking within 20 more time steps. At the point of breaking, therefore, the wave is in very shallow water, a configuration familiar enough to bodysurfers when the coast is relatively steep.

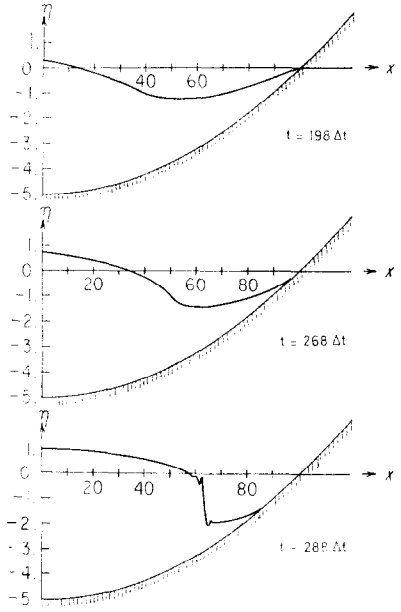

FIG. 6. Profile of an incident sine wave propagating into quiet water with a bottom of parabolic shape. The bottom has the same mean slope as in Fig. 5, and the wave parameters are the same. (Experiment 4).

Experiment 5

A more exacting test of the computational technique is that of a wave which climbs a sloping beach but does not break. If the slope is uniform, analytical solutions exist, derived by Carrier and Greenspan [4]. The initial form of this wave is given by them parametrically as follows:

$$\eta = \mu \left\{ 1 - \frac{5a^3}{3(a^2 + \sigma^2)^{3/2}} + \frac{3a^5}{2(a^2 + \sigma^2)^{5/2}} \right\}$$

$$x = -\frac{\sigma^2}{16} + \eta$$

where

$$\eta = \eta^*/\alpha L^*, \qquad \sigma^2 = 16(h^* + \eta^*)/\alpha L^*,$$

$$x = x^*/L^*, \qquad a = 1.5(1 + 0.9\mu)^{1/2}.$$

Here asterisks denote dimensional quantities, L^* is a characteristic depth, and α is the bottom slope. The origin $x = 0$ coincided with the position of the shore point at time zero. Carrier and Greenspan show that if the constant μ is less than 0.23, the wave will not break.

The development of the wave for $\mu = 0.20$ is computed by the authors and displayed in their Fig. 5 [4, p. 103]. We have reproduced their results in our computation, but because of the sensitivity of the computation in the region of the shore line, we have chosen to compare with their expanded display of the development in this region [4, Fig. 7, p. 105]. Even in this large-scale representation, Fig. 7, our results are within drafting error of the analytical solution, except for a single grid point at the shore line when the water is rising most rapidly.

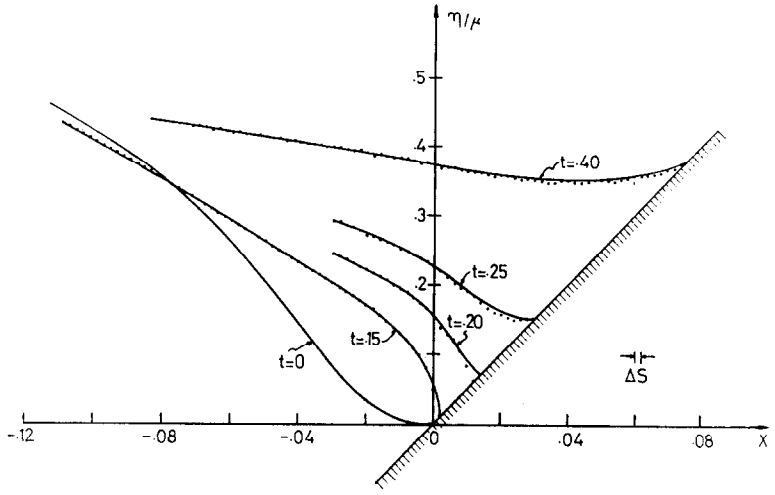

FIG. 7. Profiles of a wave climbing a beach of constant slope without breaking (after figure 7 of [4]). For specification of initial configuration, see text (Except for one point at the shore line for $t = 0.20$, the computed solution is within drafting error of the analytical solution.) (Experiment 5). ———— Analytical solution; . . . . . computed solution.

Experiment 6

It is essential to test our techniques in two dimensions as well as one. However, the only analytical solution known to us which provided a sufficiently rigorous test—including nonlinearity and a sloping bottom without lateral boundary

conditions—is that of Ball [2] for a paraboloidal basin. The initial state of the free surface is a plane displaced from equilibrium. This condition, together with the paraboloidal bottom, produces a very special nonlinear oscillation in which the free surface not only does not break, but in fact remains a plane at all times. In the absence of rotation, the surface oscillates in such a way that its normal remains in the same plane. When the coriolis term is included, the plane surface also rotates about a vertical axis, and the velocity vector, constant in space at any time, rotates about a vertical axis and oscillates in magnitude.

The shape of the basin is given by

$$h(x, y) = h_M \left[1 - \frac{x^2}{a^2} - \frac{y^2}{a^2}\right].$$

This configuration defines a frequency

$$\Omega = (2gh_M/a^2)^{1/2}$$

which, together with the coriolis frequency f, determines the frequencies of the system:

$$\omega_\pm = [\Omega^2 + \tfrac{1}{4}f^2]^{1/2} \pm \tfrac{1}{2}f.$$

For details the reader is referred to the original paper.

We have taken $a = 14$ km, $h_M = 10$ m, and $f = 10^{-3}$ sec^{-1}, which yield the periods

$$T_1 = 41.2\,\Delta t, \qquad T_2 = 107.9\,\Delta t.$$

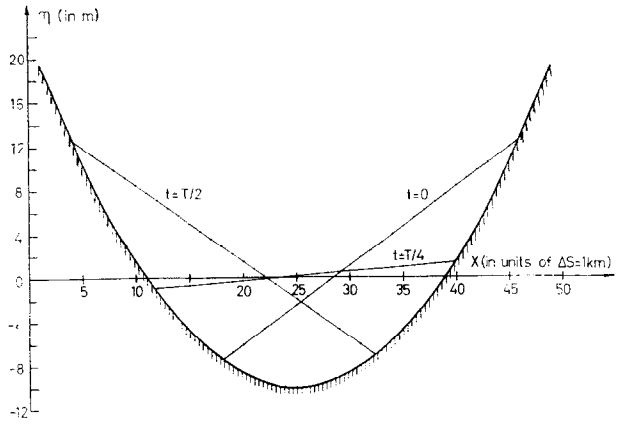

FIG. 8. Vertical section along the x-axis of paraboloidal basin

$$h = h_M\{1 - x^2/a^2 - y^2/a^2\}$$

with $h_M = 10$ m, $a = 14$ km. The position of the free surface is shown at three times. Surface remains a plane with normal in plane of paper, so that parallel sections are similar. Theoretical verification: Ball [2] (Experiment 6). ———— Analytical solution; . . . . . computed solution.

The unterrestrial value of the coriolis parameter and the shallowness of the water were partly dictated by computational economics: we have used only 49 × 49 grid points. However, the parameter values determine a highly nonlinear computation, since the maximum displacement of the surface from equilibrium is about 12 m, or 120% of the maximum depth h_M (Fig. 8). This maximum displacement is of course at the shore line, and at this point the slope of the bottom is about twice that of the free surface. Thus small errors arising out of incorrect treatment of the shoreline points would introduce perceptible wiggles into the plane free surface (see Appendix B).

The results of the computations are shown in Figs. 8 and 9. Ball gives no diagrams with which to make a comparison, and the rotating motion is not easy to visualize. We have presented in Fig. 8 a two-dimensional solution for the special case $f = 0$. Here the equations governing the x- and y-displacements are uncoupled, and the free surface remains independent of y. Figure 8 shows a vertical section through the x-axis.

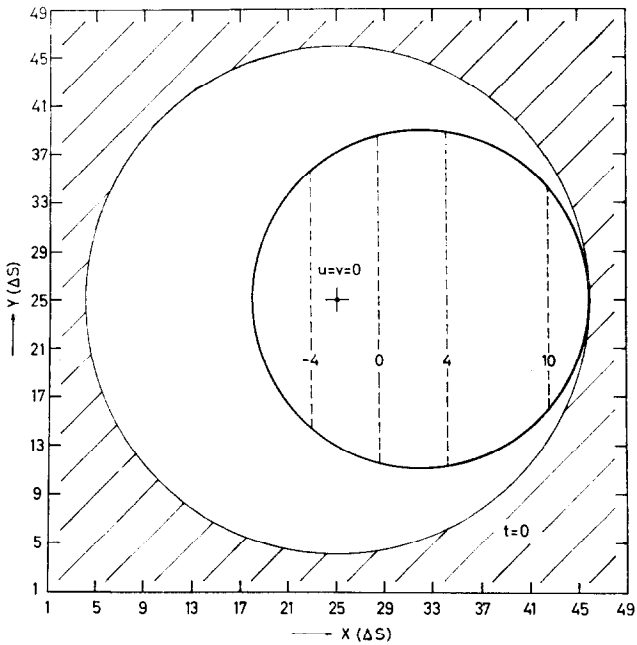

FIG. 9a. Plan form for the model of Fig. 8 but with rotation ($f = 10^{-3}$ sec^{-1}), at three times. Inner curves are the shore line ($\xi = 0$). Straight dashed lines are contours of surface elevation in meters. Outer circles are locus of high-water points. Outer squares are boundary of computational grid. Velocity vector (uniform in space) is plotted at center of basin in arbitrary units. Surface remains plane at all times. Theoretical verification: Ball [2], (Experiment 6).

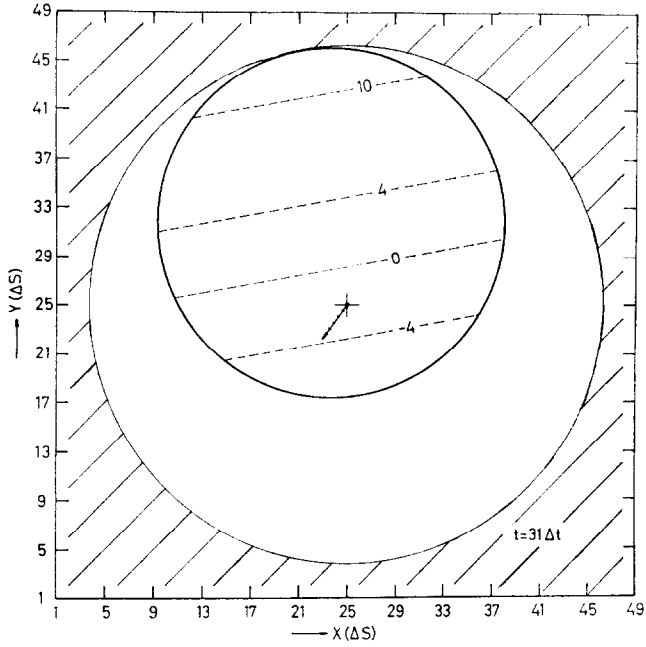

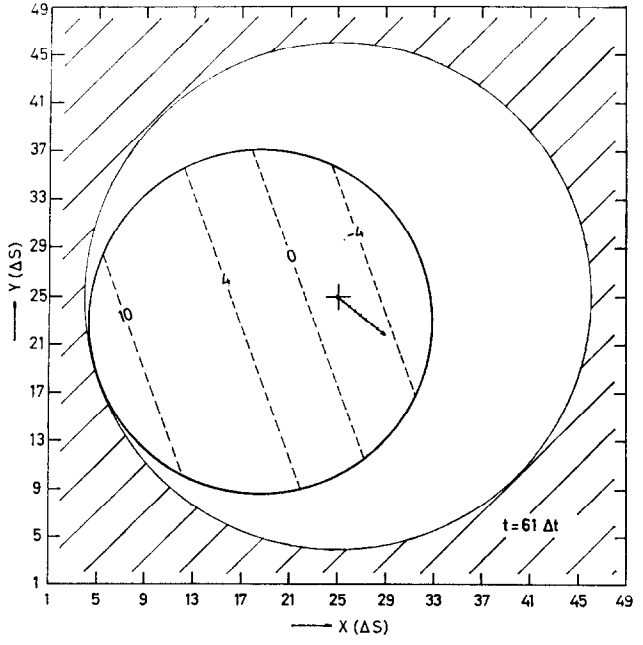

Figs. 9b, 9c.

For the rotating case (Fig. 9), we have indicated in plan form the shore line (that is, the intersection of the free surface with the basin), together with contours of elevation of the surface above equilibrium. The straightness and uniform gradient of the contours show that the surface remains a plane. The outer circle is the locus of high-water points, and the outer square is the boundary of the computing grid.

Conclusions

It is feasible to integrate the nonlinear shallow-water equations with rotation over a sloping bottom of arbitrary configuration, using any of at least three finite-difference formulations. No additional lateral boundary conditions need be applied, and the position of the shore line is determined by the computation at each time step.

It would seem entirely possible to incorporate our two-dimensional techniques into an operational storm-surge forecast program. If so, a coast would be represented simply by specifying the bottom contours. Unwanted computational effects from artificial boundaries can be avoided, and the computation of the water movement up the shore could be of especial importance in very flat coastal areas.

APPENDIX A. Finite Difference Schemes

To facilitate the conversion of Eqs. (1) into a finite difference system, it is convenient to write these equations by introducing the momentum components

$$u^* = \xi u,$$

$$v^* = \xi v.$$

Then

$$\frac{\partial \xi}{\partial t} + \frac{\partial u^*}{\partial x} + \frac{\partial v^*}{\partial y} = 0,$$

$$\frac{\partial u^*}{\partial t} + \frac{\partial}{\partial x}(u^* u + G\xi^2) + \frac{\partial}{\partial y}(v^* u) - f v^* = g\xi \frac{\partial h}{\partial x}, \tag{A.1}$$

$$\frac{\partial v^*}{\partial t} + \frac{\partial}{\partial x}(u^* v) + \frac{\partial}{\partial y}(v^* v + G\xi^2) + f u^* = g\xi \frac{\partial h}{\partial y}.$$

We have used the symbol G to denote half of the acceleration due to gravity ($G = g/2$).

Using a rectangular, nonstaggered grid, the Lax–Wendroff analog to system (A.1) becomes (Scheme I):

$$\xi_{j,k}^{n+1} = \bar{\xi}_{j,k}^{n} - \epsilon\{\Delta_j u_{j,k}^{*} + \Delta_k v_{j,k}^{*}\},$$

$$u_{j,k}^{*n+1} = \bar{u}_{j,k}^{*n} - \epsilon\left\{\Delta_j\left[\frac{(u_{j,k}^{*n})^2}{\xi_{j,k}^{n}}\right] + G\Delta_j[(\xi_{j,k}^{n})^2] + \Delta_k\left[\frac{u_{j,k}^{*n} v_{j,k}^{*n}}{\xi_{j,k}^{n}}\right]\right\}$$

$$+ f\,\Delta t\, v_{j,k}^{*n} + \epsilon g \xi_{j,k}^{n-1}\Delta_j h_{j,k},$$

$$v_{j,k}^{*n+1} = \bar{v}_{j,k}^{*n} - \epsilon\left\{\Delta_j\left[\frac{u_{j,k}^{*n} v_{j,k}^{*n}}{\xi_{j,k}^{n}}\right] + \Delta_k\left[\frac{(v_{j,k}^{*n})^2}{\xi_{j,k}^{n}}\right] + G\Delta_k[(\xi_{j,k}^{n})^2]\right\}$$

$$- f\,\Delta t\, u_{j,k}^{*n} + \epsilon g \xi_{j,k}^{n-1}\Delta_k h_{j,k},$$

followed by a second step of the form:

$$\xi_{j,k}^{n+2} = \xi_{j,k}^{n} - 2\epsilon\{\Delta_j u_{j,k}^{*n+1} + \Delta_k v_{j,k}^{*n+1}\},$$

$$u_{j,k}^{*n+2} = u_{j,k}^{*n} - 2\epsilon\left\{\Delta_j\left[\frac{(u_{j,k}^{*n+1})^2}{\xi_{j,k}^{n+1}}\right] + G\Delta_j[(\xi_{j,k}^{n+1})^2] + \Delta_k\left[\frac{u_{j,k}^{*n+1} v_{j,k}^{*n+1}}{\xi_{j,k}^{n+1}}\right]\right\}$$

$$+ 2f\,\Delta t\, v_{j,k}^{*n+1} + 2\epsilon g \xi_{j,k}^{n}\Delta_j h_{j,k},$$

$$v_{j,k}^{*n+2} = v_{j,k}^{*n} - 2\epsilon\left\{\Delta_j\left[\frac{u_{j,k}^{*n+1} v_{j,k}^{*n+1}}{\xi_{j,k}^{n+1}}\right] + \Delta_k\left[\frac{(v_{j,k}^{*n+1})^2}{\xi_{j,k}^{n+1}}\right] + G\Delta_k[(\xi_{j,k}^{n+1})^2]\right\}$$

$$- 2f\,\Delta t\, u_{j,k}^{*n+1} + 2\epsilon g \xi_{j,k}^{n}\Delta_k h_{j,k}.$$

All parameters are defined as before, and for any variable ϕ

$$\Delta_j \phi_{j,k}^{n} = \phi_{j+1,k}^{n} - \phi_{j-1,k}^{n},$$

$$\Delta_k \phi_{j,k}^{n} = \phi_{j,k+1}^{n} - \phi_{j,k-1}^{n}, \tag{A.2}$$

$$\bar{\phi}_{j,k}^{n} = \tfrac{1}{4}(\phi_{j+1,k}^{n} + \phi_{j-1,k}^{n} + \phi_{j,k+1}^{n} + \phi_{j,k-1}^{n}).$$

The indices (j, k, n) denote a point $(x, y, t) = (j\,\Delta x, k\,\Delta y, n\,\Delta t)$ of a discrete grid whose mesh size is determined by $\Delta x = \Delta y = \Delta s$ and Δt. The ratio of these increments is given by $\epsilon = \Delta t/2\,\Delta s$.

Following Arakawa's formulation [4], it is also possible to approximate Eqs. (A.1) by:

$$\xi^{n+1}_{j+1/2,k+1/2} = \xi^{n}_{j+1/2,k+1/2} - 2\epsilon\{\Delta_j u^{*n}_{j+1/2,k+1/2} + \Delta_k v^{*n}_{j+1/2,k+1/2}\}$$

$$(\bar{\xi}^{n+1}_{j,k}\tilde{u}^{n+1}_{j,k}) = (\bar{\xi}^{n}_{j,k}u^{n}_{j,k}) - 2\epsilon\{\Delta_j(\overline{U}^{*n}_{j,k}\delta_j u^{n}_{j,k} + G\delta_k[(\xi^{n+1}_{j,k})^2])$$
$$+ \Delta_k(\overline{V}^{*n}_{j,k}\{\delta_k u^{n}_{j,k}\})\} + \bar{\xi}^{n+1}_{j,k}\{f\Delta t\, v^{n}_{j,k} + 2\epsilon g\Delta_j h_{j,k}\}$$

$$(\bar{\xi}^{n+1}_{j,k}\tilde{v}^{n+1}_{j,k}) = (\bar{\xi}^{n}_{j,k}v^{n}_{j,k}) - 2\epsilon\{\Delta_j(\tilde{\overline{U}}^{*n+1}_{j,k}\delta_j v^{n}_{j,k}) + \Delta_k(\overline{V}^{*n}_{j,k}\delta_k v^{n}_{j,k} + G\delta_j[(\xi^{n+1}_{j,k})^2])\}$$
$$+ \bar{\xi}^{n+1}_{j,k}\{-f\Delta t\, \tilde{u}^{n+1}_{j,k} + 2\epsilon g\Delta_k h_{j,k}\}$$

followed by a second step for the velocity equations of the form:

$$(\bar{\xi}^{n+1}_{j,k}u^{n+1}_{j,k}) = (\bar{\xi}^{n}_{j,k}u^{n}_{j,k}) - 2\epsilon\{\Delta_j(\overline{U}^{*n}_{j,k}\delta_j\tilde{u}^{n+1}_{j,k} + G\delta_k[(\xi^{n+1}_{j,k})^2]) + \Delta_k(\overline{V}^{*n}_{j,k}\delta_k\tilde{u}^{n+1}_{j,k})\}$$
$$+ \bar{\xi}^{n+1}_{j,k}\{f\Delta t\,\tilde{v}^{n+1}_{j,k} + 2\epsilon g\Delta_j h_{j,k}\},$$

$$(\bar{\xi}^{n+1}_{j,k}v^{n+1}_{j,k}) = (\bar{\xi}^{n}_{j,k}v^{n}_{j,k}) - 2\epsilon\{\Delta_j(\tilde{\overline{U}}^{*n+1}_{j,k}\delta_j\tilde{v}^{n+1}_{j,k}) + \Delta_k(\overline{V}^{*n}_{j,k}\delta_k\tilde{v}^{n+1}_{j,k} + G\delta_j[(\xi^{n+1}_{j,k})^2])\}$$
$$+ \bar{\xi}^{n+1}_{j,k}\{f\Delta t\, u^{n+1}_{j,k} + 2\epsilon g\Delta_k h_{j,k}\}.$$

In the above equations, $\xi^{n+1}_{j,k}$, $u^{n+1}_{j,k}$, $v^{n+1}_{j,k}$ are the final values of the fields at time step $(n+1)$. The symbol $\sim$ over a variable (e.g., $\tilde{\phi}$) indicates that this is only a temporary value obtained at the first step of the numerical integration. The following definitions were introduced;

$$\Delta_j\phi^{n}_{j,k} = \phi^{n}_{j+1/2,k} - \phi^{n}_{j-1/2,k}$$

$$\Delta_k\phi^{n}_{j,k} = \phi^{n}_{j,k+1/2} - \phi^{n}_{j,k-1/2}$$

$$\delta_j\phi^{n}_{j,k} = \tfrac{1}{2}(\phi^{n}_{j+1/2,k} + \phi^{n}_{j-1/2,k})$$

$$\delta_k\phi^{n}_{j,k} = \tfrac{1}{2}(\phi^{n}_{j,k+1/2} + \phi^{n}_{j,k-1/2})$$

$$u^{*}_{j,k+1/2} = (\delta_j\xi_{j,k+1/2})(\delta_k u_{j,k+1/2})$$

$$v^{*}_{j+1/2,k} = (\delta_k\xi_{j+1/2,k})(\delta_j v_{j+1/2,k})$$

$$\overline{U}^{*}_{j+1/2,k} = \tfrac{1}{2}(\delta_j u^{*}_{j+1/2,k+1/2} + \delta_j u^{*}_{j+1/2,k-1/2})$$

$$\overline{V}^{*}_{j,k+1/2} = \tfrac{1}{2}(\delta_k v^{*}_{j-1/2,k+1/2} + \delta_k v^{*}_{j+1/2,k+1/2})$$

$$\bar{\xi}_{j,k} = \tfrac{1}{2}(\delta_j\xi_{j,k+1/2} + \delta_j\xi_{j,k-1/2}).$$

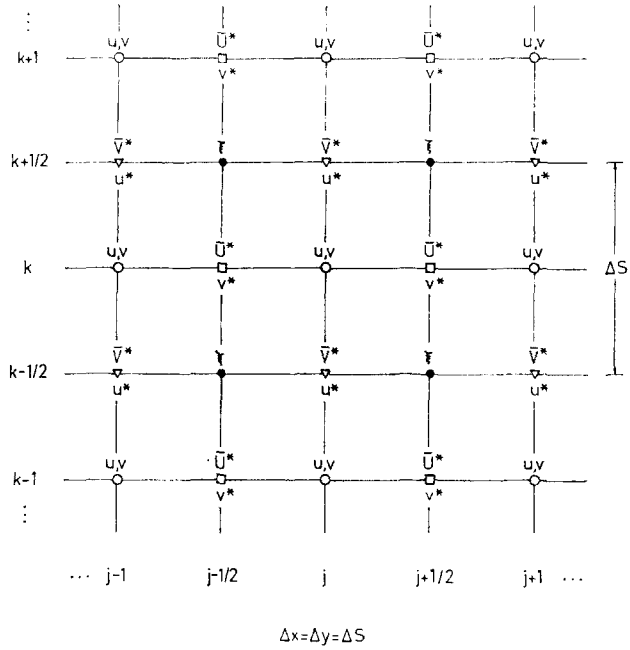

FIG. 10. Grid for Scheme II (Appendix A).

The grid used for this system is displayed in Fig. 10. In the text we have referred to this finite difference representation as Scheme II.

Finally, it is also possible to generalize a relatively simpler scheme whose properties for linearized problems have been studied in detail [10]. In this case, we approximate Eqs. (1) by:

$$\eta_{j,k}^{n+1} = \eta_{j,k}^{n} - \epsilon\{\Delta_j([h_{j,k} + \eta_{j,k}^{n}]\, u_{j,k}^{n}) + \Delta_k([h_{j,k} + \eta_{j,k}^{n}]\, v_{j,k}^{n})\}$$

$$u_{j,k}^{n+1} = u_{j,k}^{n}\{1 - \epsilon\Delta_j u_{j,k}^{n}\} + v_{j,k}^{n}\{f\,\Delta t - \epsilon\Delta_k u_{j,k}^{n}\} - g\epsilon\Delta_j \eta_{j,k}^{n+1}$$

$$v_{j,k}^{n+1} = v_{j,k}^{n}\{1 - \epsilon\Delta_k v_{j,k}^{n}\} + u_{j,k}^{n+1}\{-f\,\Delta t - \epsilon\Delta_j v_{j,k}^{n}\} - g\epsilon\Delta_k \eta_{j,k}^{n+1},$$

followed by a second step for the velocity equations of the form:

$$\overset{\infty}{u}{}_{j,k}^{n+1} = u_{j,k}^{n}\{1 - \epsilon\Delta_j u_{j,k}^{n+1}\} - \epsilon v_{j,k}^{n}\Delta_k u_{j,k}^{n+1} + f\,\Delta t\, v_{j,k}^{n+1} - g\epsilon\Delta_j \eta_{j,k}^{n+1},$$

$$\overset{\infty}{v}{}_{j,k}^{n+1} = v_{j,k}^{n}\{1 - \epsilon\Delta_k v_{j,k}^{n+1}\} - \epsilon u_{j,k}^{n+1}\Delta_j v_{j,k}^{n+1} - f\,\Delta t\, \overset{\infty}{u}{}_{j,k}^{n+1} - g\epsilon\Delta_k \eta_{j,k}^{n+1}.$$

$\eta_{j,k}^{n+1}$, $\overset{\infty}{u}{}_{j,k}^{n+1}$, and $\overset{\infty}{v}{}_{j,k}^{n+1}$ represent the final values of the fields at time $(n+1)\,\Delta t$.

Other symbols are used according to definition (A.2). This system, referred to as Scheme III, was used with a nonstaggered grid of mesh size Δs, Δt, and as before $\epsilon = \Delta t/2\,\Delta s$.

Appendix B. Treatment of Shore-Line Points

No difficulty whatever is encountered when the water is receding down the shore. However, when it is rising, a new underground point may enter the field at any time step. To compute the position of the new shore line, it is necessary to know the slope of the free surface at the present shore line, which of course does not, in general, coincide with a grid point. The use of a zero value for ξ at the first underground point will produce a kink in the free surface at the first underwater point, and the ensuing convergence at that point will cause an artificial rise in the surface, appearing as a small-scale wiggle. Since no smoothing operators are used in our computation, such wiggles would quickly propagate inward and contaminate the results.

To prevent this, we estimate the slope of the free surface at the shore line by an extrapolation from the last two underwater points to the first underground point. In detail, the procedure is as follows.

1. To determine the shore line, given a field of ξ, search outward from deep water until the first point is reached for which $\xi < \delta$, where δ is some small positive quantity determined by the accuracy of the computation. (We used $\delta = 10^{-6}$.) This is called the first underground point, denoted by $J + 1$ in Fig. 11. The last underwater point is then J.

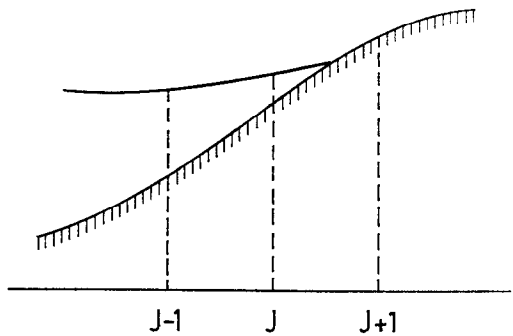

Fig. 11. Technique of treating shore-line points (Appendix B).

2. u is computed at underwater points only and at underground points is set to zero.

3. If ξ^n_{J+1} is the first underground point at time step n, then ξ^{n+1}_{J+1} is computed using: (i) a value of ξ^n_{J+1} given by the linear extrapolation of ξ^n from $J-1$ and J; and (ii) a one-sided difference of momentum with u^n_{J+1} given by the linear extrapolation of u^n from $J-1$ and J.

Then symbolically,

$$\xi^{n+1}_{J+1} = [\xi^n_{J+1}]_{\text{extrap}} - \frac{\Delta t}{\Delta s}\{[\xi^n_{J+1} u^n_{J+1}]_{\text{extrap}} - \xi^n_J u^n_J\}.$$

The procedure above is that for one dimension. In two dimensions the logic of the program becomes more complicated, but the principles are the same.

ACKNOWLEDGMENTS

We wish to thank Professor A. Arakawa for his helpful advice with regard to Scheme II.

Financial support for the research was provided under E.S.S.A. Contract Cwb 11207 and N.S.F. G10167.

The computations were carried out in part in the Campus Computing Network of U.C.L.A., for whose cooperation we are grateful.

REFERENCES

1. J. J. STOKER, "Water Waves." Interscience, New York, 1957.
2. F. K. BALL, An exact theory of simple finite shallow water oscillations of a rotating earth. *Proc. 1st Austral. Conf. Hydraulics and Fluid Mech., 1962.* Pergamon, 1964.
3. J. J. STOKER, The formation of breakers and bores. *Commun. Pure Appl. Math.* **1** (1948), 1.
4. G. CARRIER AND H. GREENSPAN, Water waves of finite amplitude on a sloping beach, *J. Fluid Mech.* **4** (1958), 97.
5. G. W. PLATZMAN, The dynamic prediction of wind tides on Lake Erie, *Meteorol. Monogr.* **4** (1963), No. 26.
6. R. O. REID AND B. R. BODINE, Numerical model for storm surges in Galveston Bay, *Proc. Amer. Soc. Civil. Eng. J. Waterways Harbors Div.* **94** (1968), 33.
7. R. RICHTMYER, A surrey of finite difference methods for non-steady fluid dynamics, NCAR Tech. Note 63–2 (1963).
8. D. HOUGHTON AND A. KASAHARA, Non-linear shallow-fluid flow over an isolated ridge, *Commun. Pure Appl. Math.* **21** (1968), 1.
9. A. ARAKAWA, Computational design for long-term numerical integration of the equations of fluid motion: two-dimensional incompressible flow, *J. Comput. Phys.* **1** (1966), 143.
10. A. SIELECKI, An energy-conserving difference scheme for the storm-surge equations, *Mon. Weather Rev.* **96** (1968), 150.